

# $J/\psi$ Production in Au-Au Collisions at $\sqrt{s_{NN}} = 200$ GeV

S.S. Adler,<sup>5</sup> S. Afanasiev,<sup>17</sup> C. Aidala,<sup>5</sup> N.N. Ajitanand,<sup>43</sup> Y. Akiba,<sup>20,38</sup> J. Alexander,<sup>43</sup> R. Amirikas,<sup>12</sup> L. Aphecetche,<sup>45</sup> S.H. Aronson,<sup>5</sup> R. Averbeck,<sup>44</sup> T.C. Awes,<sup>35</sup> R. Azmoun,<sup>44</sup> V. Babintsev,<sup>15</sup> A. Baldisseri,<sup>10</sup> K.N. Barish,<sup>6</sup> P.D. Barnes,<sup>27</sup> B. Bassalleck,<sup>33</sup> S. Bathe,<sup>30</sup> S. Batsouli,<sup>9</sup> V. Baublis,<sup>37</sup> A. Bazilevsky,<sup>39,15</sup> S. Belikov,<sup>16,15</sup> Y. Berdnikov,<sup>40</sup> S. Bhagavatula,<sup>16</sup> J.G. Boissevain,<sup>27</sup> H. Borel,<sup>10</sup> S. Borenstein,<sup>25</sup> M.L. Brooks,<sup>27</sup> D.S. Brown,<sup>34</sup> N. Bruner,<sup>33</sup> D. Bucher,<sup>30</sup> H. Buesching,<sup>30</sup> V. Bumazhnov,<sup>15</sup> G. Bunce,<sup>5,39</sup> J.M. Burward-Hoy,<sup>26,44</sup> S. Butsyk,<sup>44</sup> X. Camard,<sup>45</sup> J.-S. Chai,<sup>18</sup> P. Chand,<sup>4</sup> W.C. Chang,<sup>2</sup> S. Chernichenko,<sup>15</sup> C.Y. Chi,<sup>9</sup> J. Chiba,<sup>20</sup> M. Chiu,<sup>9</sup> I.J. Choi,<sup>52</sup> J. Choi,<sup>19</sup> R.K. Choudhury,<sup>4</sup> T. Chujo,<sup>5</sup> V. Cianciolo,<sup>35</sup> Y. Cobigo,<sup>10</sup> B.A. Cole,<sup>9</sup> P. Constantin,<sup>16</sup> D.G. d'Enterria,<sup>45</sup> G. David,<sup>5</sup> H. Delagrange,<sup>45</sup> A. Denisov,<sup>15</sup> A. Deshpande,<sup>39</sup> E.J. Desmond,<sup>5</sup> O. Dietzsch,<sup>41</sup> O. Drapier,<sup>25</sup> A. Drees,<sup>44</sup> R. du Rietz,<sup>29</sup> A. Durum,<sup>15</sup> D. Dutta,<sup>4</sup> Y.V. Efremenko,<sup>35</sup> K. El Chenawi,<sup>49</sup> A. Enokizono,<sup>14</sup> H. En'yo,<sup>38,39</sup> S. Esumi,<sup>48</sup> L. Ewell,<sup>5</sup> D.E. Fields,<sup>33,39</sup> F. Fleuret,<sup>25</sup> S.L. Fokin,<sup>23</sup> B.D. Fox,<sup>39</sup> Z. Fraenkel,<sup>51</sup> J.E. Frantz,<sup>9</sup> A. Franz,<sup>5</sup> A.D. Frawley,<sup>12</sup> S.-Y. Fung,<sup>6</sup> S. Garpman,<sup>29,\*</sup> T.K. Ghosh,<sup>49</sup> A. Glenn,<sup>46</sup> G. Gogiberidze,<sup>46</sup> M. Gonin,<sup>25</sup> J. Gosset,<sup>10</sup> Y. Goto,<sup>39</sup> R. Granier de Cassagnac,<sup>25</sup> N. Grau,<sup>16</sup> S.V. Greene,<sup>49</sup> M. Grosse Perdekamp,<sup>39</sup> W. Guryn,<sup>5</sup> H.-Å. Gustafsson,<sup>29</sup> T. Hachiya,<sup>14</sup> J.S. Haggerty,<sup>5</sup> H. Hamagaki,<sup>8</sup> A.G. Hansen,<sup>27</sup> E.P. Hartouni,<sup>26</sup> M. Harvey,<sup>5</sup> R. Hayano,<sup>8</sup> X. He,<sup>13</sup> M. Heffner,<sup>26</sup> T.K. Hemmick,<sup>44</sup> J.M. Heuser,<sup>44</sup> M. Hibino,<sup>50</sup> J.C. Hill,<sup>16</sup> W. Holzmann,<sup>43</sup> K. Homma,<sup>14</sup> B. Hong,<sup>22</sup> A. Hoover,<sup>34</sup> T. Ichihara,<sup>38,39</sup> V.V. Ikonnikov,<sup>23</sup> K. Imai,<sup>24,38</sup> L.D. Isenhower,<sup>1</sup> M. Ishihara,<sup>38</sup> M. Issah,<sup>43</sup> A. Isupov,<sup>17</sup> B.V. Jacak,<sup>44</sup> W.Y. Jang,<sup>22</sup> Y. Jeong,<sup>19</sup> J. Jia,<sup>44</sup> O. Jinnouchi,<sup>38</sup> B.M. Johnson,<sup>5</sup> S.C. Johnson,<sup>26</sup> K.S. Joo,<sup>31</sup> D. Jouan,<sup>36</sup> S. Kametani,<sup>8,50</sup> N. Kamihara,<sup>47,38</sup> J.H. Kang,<sup>52</sup> S.S. Kapoor,<sup>4</sup> K. Katou,<sup>50</sup> S. Kelly,<sup>9</sup> B. Khachaturov,<sup>51</sup> A. Khanzadeev,<sup>37</sup> J. Kikuchi,<sup>50</sup> D.H. Kim,<sup>31</sup> D.J. Kim,<sup>52</sup> D.W. Kim,<sup>19</sup> E. Kim,<sup>42</sup> G.-B. Kim,<sup>25</sup> H.J. Kim,<sup>52</sup> E. Kistenev,<sup>5</sup> A. Kiyomichi,<sup>48</sup> K. Kiyoyama,<sup>32</sup> C. Klein-Boesing,<sup>30</sup> H. Kobayashi,<sup>38,39</sup> L. Kochenda,<sup>37</sup> V. Kochetkov,<sup>15</sup> D. Koehler,<sup>33</sup> T. Kohama,<sup>14</sup> M. Kopytine,<sup>44</sup> D. Kotchetkov,<sup>6</sup> A. Kozlov,<sup>51</sup> P.J. Kroon,<sup>5</sup> C.H. Kuberg,<sup>1,27</sup> K. Kurita,<sup>39</sup> Y. Kuroki,<sup>48</sup> M.J. Kweon,<sup>22</sup> Y. Kwon,<sup>52</sup> G.S. Kyle,<sup>34</sup> R. Lacey,<sup>43</sup> V. Ladygin,<sup>17</sup> J.G. Lajoie,<sup>16</sup> A. Lebedev,<sup>16,23</sup> S. Leckey,<sup>44</sup> D.M. Lee,<sup>27</sup> S. Lee,<sup>19</sup> M.J. Leitch,<sup>27</sup> X.H. Li,<sup>6</sup> H. Lim,<sup>42</sup> A. Litvinenko,<sup>17</sup> M.X. Liu,<sup>27</sup> Y. Liu,<sup>36</sup> C.F. Maguire,<sup>49</sup> Y.I. Makdisi,<sup>5</sup> A. Malakhov,<sup>17</sup> V.I. Manko,<sup>23</sup> Y. Mao,<sup>7,38</sup> G. Martinez,<sup>45</sup> M.D. Marx,<sup>44</sup> H. Masui,<sup>48</sup> F. Matathias,<sup>44</sup> T. Matsumoto,<sup>8,50</sup> P.L. McGaughey,<sup>27</sup> E. Melnikov,<sup>15</sup> F. Messer,<sup>44</sup> Y. Miake,<sup>48</sup> J. Milan,<sup>43</sup> T.E. Miller,<sup>49</sup> A. Milov,<sup>44,51</sup> S. Mioduszewski,<sup>5</sup> R.E. Mischke,<sup>27</sup> G.C. Mishra,<sup>13</sup> J.T. Mitchell,<sup>5</sup> A.K. Mohanty,<sup>4</sup> D.P. Morrison,<sup>5</sup> J.M. Moss,<sup>27</sup> F. Mühlbacher,<sup>44</sup> D. Mukhopadhyay,<sup>51</sup> M. Muniruzzaman,<sup>6</sup> J. Murata,<sup>38,39</sup> S. Nagamiya,<sup>20</sup> J.L. Nagle,<sup>9</sup> T. Nakamura,<sup>14</sup> B.K. Nandi,<sup>6</sup> M. Nara,<sup>48</sup> J. Newby,<sup>46</sup> P. Nilsson,<sup>29</sup> A.S. Nyanin,<sup>23</sup> J. Nystrand,<sup>29</sup> E. O'Brien,<sup>5</sup> C.A. Ogilvie,<sup>16</sup> H. Ohnishi,<sup>5,38</sup> I.D. Ojha,<sup>49,3</sup> K. Okada,<sup>38</sup> M. Ono,<sup>48</sup> V. Onuchin,<sup>15</sup> A. Oskarsson,<sup>29</sup> I. Otterlund,<sup>29</sup> K. Oyama,<sup>8</sup> K. Ozawa,<sup>8</sup> D. Pal,<sup>51</sup> A.P.T. Palounek,<sup>27</sup> V.S. Pantuev,<sup>44</sup> V. Papavassiliou,<sup>34</sup> J. Park,<sup>42</sup> A. Parmar,<sup>33</sup> S.F. Pate,<sup>34</sup> T. Peitzmann,<sup>30</sup> J.-C. Peng,<sup>27</sup> V. Peresedov,<sup>17</sup> C. Pinkenburg,<sup>5</sup> R.P. Pisani,<sup>5</sup> F. Plasil,<sup>35</sup> M.L. Purschke,<sup>5</sup> A. Purwar,<sup>44</sup> J. Rak,<sup>16</sup> I. Ravinovich,<sup>51</sup> K.F. Read,<sup>35,46</sup> M. Reuter,<sup>44</sup> K. Reygers,<sup>30</sup> V. Riabov,<sup>37,40</sup> Y. Riabov,<sup>37</sup> G. Roche,<sup>28</sup> A. Romana,<sup>25</sup> M. Rosati,<sup>16</sup> P. Rosnet,<sup>28</sup> S.S. Ryu,<sup>52</sup> M.E. Sadler,<sup>1</sup> N. Saito,<sup>38,39</sup> T. Sakaguchi,<sup>8,50</sup> M. Sakai,<sup>32</sup> S. Sakai,<sup>48</sup> V. Samsonov,<sup>37</sup> L. Sanfratello,<sup>33</sup> R. Santo,<sup>30</sup> H.D. Sato,<sup>24,38</sup> S. Sato,<sup>5,48</sup> S. Sawada,<sup>20</sup> Y. Schutz,<sup>45</sup> V. Semenov,<sup>15</sup> R. Seto,<sup>6</sup> M.R. Shaw,<sup>1,27</sup> T.K. Shea,<sup>5</sup> T.-A. Shibata,<sup>47,38</sup> K. Shigaki,<sup>14,20</sup> T. Shiina,<sup>27</sup> C.L. Silva,<sup>41</sup> D. Silvermyr,<sup>27,29</sup> K.S. Sim,<sup>22</sup> C.P. Singh,<sup>3</sup> V. Singh,<sup>3</sup> M. Sivertz,<sup>5</sup> A. Soldatov,<sup>15</sup> R.A. Soltz,<sup>26</sup> W.E. Sondheim,<sup>27</sup> S.P. Sorensen,<sup>46</sup> I.V. Sourikova,<sup>5</sup> F. Staley,<sup>10</sup> P.W. Stankus,<sup>35</sup> E. Stenlund,<sup>29</sup> M. Stepanov,<sup>34</sup> A. Ster,<sup>21</sup> S.P. Stoll,<sup>5</sup> T. Sugitate,<sup>14</sup> J.P. Sullivan,<sup>27</sup> E.M. Takagui,<sup>41</sup> A. Taketani,<sup>38,39</sup> M. Tamai,<sup>50</sup> K.H. Tanaka,<sup>20</sup> Y. Tanaka,<sup>32</sup> K. Tanida,<sup>38</sup> M.J. Tannenbaum,<sup>5</sup> P. Tarján,<sup>11</sup> J.D. Tepe,<sup>1,27</sup> T.L. Thomas,<sup>33</sup> J. Tojo,<sup>24,38</sup> H. Torii,<sup>24,38</sup> R.S. Towell,<sup>1</sup> I. Tseruya,<sup>51</sup> H. Tsuruoka,<sup>48</sup> S.K. Tuli,<sup>3</sup> H. Tydesjö,<sup>29</sup> N. Tyurin,<sup>15</sup> H.W. van Hecke,<sup>27</sup> J. Velkovska,<sup>5,44</sup> M. Velkovsky,<sup>44</sup> L. Villatte,<sup>46</sup> A.A. Vinogradov,<sup>23</sup> M.A. Volkov,<sup>23</sup> E. Vznuzdaev,<sup>37</sup> X.R. Wang,<sup>13</sup> Y. Watanabe,<sup>38,39</sup> S.N. White,<sup>5</sup> F.K. Wohn,<sup>16</sup> C.L. Woody,<sup>5</sup> W. Xie,<sup>6</sup> Y. Yang,<sup>7</sup> A. Yanovich,<sup>15</sup> S. Yokkaichi,<sup>38,39</sup> G.R. Young,<sup>35</sup> I.E. Yushmanov,<sup>23</sup> W.A. Zajc,<sup>9,†</sup> C. Zhang,<sup>9</sup> S. Zhou,<sup>7,51</sup> and L. Zolin<sup>17</sup>

(PHENIX Collaboration)

<sup>1</sup>Abilene Christian University, Abilene, TX 79699, USA

<sup>2</sup>Institute of Physics, Academia Sinica, Taipei 11529, Taiwan

<sup>3</sup>Department of Physics, Banaras Hindu University, Varanasi 221005, India

<sup>4</sup>Bhabha Atomic Research Centre, Bombay 400 085, India

<sup>5</sup>Brookhaven National Laboratory, Upton, NY 11973-5000, USA

<sup>6</sup>University of California - Riverside, Riverside, CA 92521, USA

<sup>7</sup>China Institute of Atomic Energy (CIAE), Beijing, Peoples Republic of China

- <sup>8</sup>Center for Nuclear Study, Graduate School of Science, University of Tokyo, 7-3-1 Hongo, Bunkyo, Tokyo 113-0033, Japan  
<sup>9</sup>Columbia University, New York, NY 10027 and Nevis Laboratories, Irvington, NY 10533, USA  
<sup>10</sup>Dapnia, CEA Saclay, Bat. 703, F-91191, Gif-sur-Yvette, France  
<sup>11</sup>Debrecen University, H-4010 Debrecen, Egyetem tér 1, Hungary  
<sup>12</sup>Florida State University, Tallahassee, FL 32306, USA  
<sup>13</sup>Georgia State University, Atlanta, GA 30303, USA  
<sup>14</sup>Hiroshima University, Kagamiyama, Higashi-Hiroshima 739-8526, Japan  
<sup>15</sup>Institute for High Energy Physics (IHEP), Protvino, Russia  
<sup>16</sup>Iowa State University, Ames, IA 50011, USA  
<sup>17</sup>Joint Institute for Nuclear Research, 141980 Dubna, Moscow Region, Russia  
<sup>18</sup>KAERI, Cyclotron Application Laboratory, Seoul, South Korea  
<sup>19</sup>Kangnung National University, Kangnung 210-702, South Korea  
<sup>20</sup>KEK, High Energy Accelerator Research Organization, Tsukuba-shi, Ibaraki-ken 305-0801, Japan  
<sup>21</sup>KFKI Research Institute for Particle and Nuclear Physics (RMKI), H-1525 Budapest 114, POBox 49, Hungary  
<sup>22</sup>Korea University, Seoul, 136-701, Korea  
<sup>23</sup>Russian Research Center “Kurchatov Institute”, Moscow, Russia  
<sup>24</sup>Kyoto University, Kyoto 606, Japan  
<sup>25</sup>Laboratoire Leprince-Ringuet, Ecole Polytechnique, CNRS-IN2P3, Route de Saclay, F-91128, Palaiseau, France  
<sup>26</sup>Lawrence Livermore National Laboratory, Livermore, CA 94550, USA  
<sup>27</sup>Los Alamos National Laboratory, Los Alamos, NM 87545, USA  
<sup>28</sup>LPC, Université Blaise Pascal, CNRS-IN2P3, Clermont-Fd, 63177 Aubiere Cedex, France  
<sup>29</sup>Department of Physics, Lund University, Box 118, SE-221 00 Lund, Sweden  
<sup>30</sup>Institut fuer Kernphysik, University of Muenster, D-48149 Muenster, Germany  
<sup>31</sup>Myongji University, Yongin, Kyonggido 449-728, Korea  
<sup>32</sup>Nagasaki Institute of Applied Science, Nagasaki-shi, Nagasaki 851-0193, Japan  
<sup>33</sup>University of New Mexico, Albuquerque, NM, USA  
<sup>34</sup>New Mexico State University, Las Cruces, NM 88003, USA  
<sup>35</sup>Oak Ridge National Laboratory, Oak Ridge, TN 37831, USA  
<sup>36</sup>IPN-Orsay, Université Paris Sud, CNRS-IN2P3, BP1, F-91406, Orsay, France  
<sup>37</sup>PNPI, Petersburg Nuclear Physics Institute, Gatchina, Russia  
<sup>38</sup>RIKEN (The Institute of Physical and Chemical Research), Wako, Saitama 351-0198, JAPAN  
<sup>39</sup>RIKEN BNL Research Center, Brookhaven National Laboratory, Upton, NY 11973-5000, USA  
<sup>40</sup>St. Petersburg State Technical University, St. Petersburg, Russia  
<sup>41</sup>Universidade de São Paulo, Instituto de Física, Caixa Postal 66318, São Paulo CEP05315-970, Brazil  
<sup>42</sup>System Electronics Laboratory, Seoul National University, Seoul, South Korea  
<sup>43</sup>Chemistry Department, Stony Brook University, SUNY, Stony Brook, NY 11794-3400, USA  
<sup>44</sup>Department of Physics and Astronomy, Stony Brook University, SUNY, Stony Brook, NY 11794, USA  
<sup>45</sup>SUBATECH (Ecole des Mines de Nantes, CNRS-IN2P3, Université de Nantes) BP 20722 - 44307, Nantes, France  
<sup>46</sup>University of Tennessee, Knoxville, TN 37996, USA  
<sup>47</sup>Department of Physics, Tokyo Institute of Technology, Tokyo, 152-8551, Japan  
<sup>48</sup>Institute of Physics, University of Tsukuba, Tsukuba, Ibaraki 305, Japan  
<sup>49</sup>Vanderbilt University, Nashville, TN 37235, USA  
<sup>50</sup>Waseda University, Advanced Research Institute for Science and Engineering, 17 Kikui-cho, Shinjuku-ku, Tokyo 162-0044, Japan  
<sup>51</sup>Weizmann Institute, Rehovot 76100, Israel  
<sup>52</sup>Yonsei University, IPAP, Seoul 120-749, Korea
- (Dated: July 15, 2021)

First results on charm quarkonia production in heavy ion collisions at the Relativistic Heavy Ion Collider (RHIC) are presented. The yield of  $J/\psi$ 's measured in the PHENIX experiment via electron-positron decay pairs at mid-rapidity for Au-Au reactions at  $\sqrt{s_{NN}} = 200$  GeV are analyzed as a function of collision centrality. For this analysis we have studied 49.3 million minimum bias Au-Au reactions. We present the  $J/\psi$  invariant yield  $dN/dy$  for peripheral and mid-central reactions. For the most central collisions where we observe no signal above background, we quote 90% confidence level upper limits. We compare these results with our  $J/\psi$  measurement from proton-proton reactions at the same energy. We find that our measurements are not consistent with models that predict strong enhancement relative to binary collision scaling.

PACS numbers: 25.75.Dw

## I. INTRODUCTION

Lattice Quantum Chromodynamics (QCD) calculations indicate that there is a transition of nuclear matter from confined to deconfined quarks and gluons at a temperature of order  $T_c = 170$  MeV. Characteristic of this deconfined state of matter is the dynamic screening of the long-range confining potential of QCD. Color screening is predicted to reduce the attraction between heavy quark-antiquark pairs, and thus leads to a decrease in the ratio of hidden charm and beauty (quarkonia) to open charm and beauty [1, 2]. Thus, one expects a suppression of quarkonium states ( $J/\psi$ ,  $\psi'$ ,  $\chi_c$ ,  $\Upsilon(1s, 2s, 3s)$ ) depending on their binding energy and the temperature of the surrounding system.

In relativistic heavy ion collisions a state of a deconfined thermalized quark-gluon plasma may be created. Measurements in Pb-Pb reactions at  $\sqrt{s_{NN}} = 17.3$  GeV by the NA50 experiment [3] show a suppression of heavy quarkonia production relative to “normal” nuclear absorption, the dissociation of  $c\bar{c}$  pairs by interactions with the nucleons into separate quarks that eventually hadronize into  $D$  mesons [4, 5, 6, 7]. This suppression has been interpreted in the context of color screening in a quark-gluon plasma [6, 8], additional absorption with co-moving hadrons [9, 10], and multiple scattering between the charm quarks and the surrounding medium [11, 12].

At RHIC energies, where of order 10  $c\bar{c}$  pairs are produced in central Au-Au reactions [13, 14], some models predict an enhancement of heavy quarkonia due to  $c\bar{c}$  coalescence in a quark-gluon plasma [15], detailed balance of  $D + \bar{D} \leftrightarrow J/\psi + X$  [16], and/or statistical  $J/\psi$  production [17]. In addition, at RHIC energies initial state effects of shadowing and possible parton saturation may play a role in initial charm production [18]. Disentangling these competing effects will require a systematic study of yields of various quarkonium states in different colliding systems (proton-proton, proton (or deuteron)-ion, and ion-ion) and over a wide kinematic range in terms of transverse momentum and  $x_F$ .

We report here the first results on  $J/\psi$  production via electron-positron decay pairs at mid-rapidity from Au-Au collisions at  $\sqrt{s_{NN}} = 200$  GeV from data taken during Run-2 at RHIC in 2001. For peripheral and mid-central Au-Au collisions, we present the most probable yield values, while for central reactions, we observe no signal above background and thus quote 90% confidence level upper limits on  $J/\psi$  production.

## II. PHENIX EXPERIMENT

The PHENIX experiment is specifically designed to make use of high luminosity ion-ion, proton-ion, and proton-proton collisions at the Relativistic Heavy Ion Collider to sample rare physics probes including the  $J/\psi$

and other heavy quarkonium states. The PHENIX experiment includes two central rapidity spectrometer arms, each covering the pseudo-rapidity range  $|\eta| < 0.35$  and an interval of 90 degrees in azimuthal angle  $\phi$ . The spectrometers are comprised from the inner radius outward of a Multiplicity and Vertex Detector (MVD), Drift Chambers (DC), Pixel Pad Chambers (PC), Ring Imaging Cerenkov Counters (RICH), Time-of-Flight Scintillator Wall (TOF), Time Expansion Chambers (TEC), and two types of Electromagnetic Calorimeters (EMC). This combination of detectors allows for the clean identification of electrons over a broad range in transverse momentum. Further details of the detector design and performance are given in [19].

The Au-Au event centrality is estimated using the combined data from our Beam-Beam Counters (BBC) and Zero Degree Calorimeters (ZDC). While the ZDCs measure forward neutrons that result from fragmentation of the colliding nuclei, the BBCs are sensitive to charged particles produced in the collisions. Together, both detectors yield information on the impact parameter of the nuclear reaction [20]. These observables, combined with a Glauber model for the nuclear geometry, allow us to determine different collision geometry categories, referred to as centrality ranges [21].

For the analysis presented here, the electron (positron) momentum and charge sign is determined from tracking using the DC and the PC and then projecting back through the PHENIX axial magnetic field to the collision point determined by the BBC [22]. The momentum resolution achieved is  $\delta p/p = 0.7\% \oplus 1.0\% \times p$  (in GeV/c). Electrons are cleanly separated from the large background of charged pions and kaons by associating the tracks with at least three active photomultiplier tubes in the RICH [23]. In addition, we compare the track momentum ( $p$ ) to the energy ( $E$ ) measured in the Electromagnetic Calorimeter. The  $E/p$  ratio is used to further reduce the pion contamination in the electron sample. Pions typically deposit only a fraction of their energy in the calorimeter whereas electrons deposit all of their energy. These selections are augmented by requiring that the calorimeter shower position and time-of-flight information agree with the track projection. Thus, we obtain a clean sample of electron and positron candidates with less than 5% contamination.

## III. DATA SELECTION AND TRIGGERS

The Au-Au data at  $\sqrt{s_{NN}} = 200$  GeV used in this analysis were recorded during Run 2 at RHIC in the fall of 2001. For our “minimum bias” Au-Au event selection, we use a Level-1 trigger that requires a coincidence between our BBCs. We place an additional offline requirement of at least one forward neutron in each of our ZDCs to remove beam related backgrounds. Our “minimum bias” sample includes 92% of the 6.9 barn Au-Au inelastic cross section [21]. We further restrict our analy-

sis to 90% of the inelastic cross section to remove a small remaining contribution from beam related background events.

We observed a Au-Au inelastic collision rate that increased during the running period from 100 to 1200 Hz. The Level-2 triggers are implemented in a personal computer-based farm with 30 processors in Run 2, as part of the PHENIX Event Builder [19]. The Level-2  $J/\psi$  trigger algorithm identified electron candidates by starting with rings in the RICH and then searching for possible matching showers in the EMC. The EMC search window based on the RICH ring is obtained from a lookup table, generated using Monte Carlo simulations of single electrons. Possible matches were assumed to be electron candidates, and the electron momentum was taken to be the EMC shower energy. The invariant mass was calculated for all electron candidate pairs within an event, regardless of the candidate's charge sign. If the invariant mass was higher than  $2.2 \text{ GeV}/c^2$ , the pair was accepted as a  $J/\psi$  candidate, and the entire event was archived. The Level-2 trigger provided a rejection factor of order 30 relative to our "minimum bias" Level-1 trigger sample.

An additional offline requirement was imposed that the collisions have a z-vertex satisfying  $|z| < 30 \text{ cm}$  in order to eliminate collisions taking place near the PHENIX magnet. After this selection, we have analyzed 25.9 million "minimum bias" Au-Au reactions as triggered by our BBC Level-1 Trigger. In addition, from the high luminosity period of running, we also processed 23.4 million "minimum bias" events with our  $J/\psi$  Level-2 trigger.

#### IV. $J/\psi$ SIGNAL COUNTING

For three exclusive centrality bins, 0-20%, 20-40%, and 40-90% of the total Au-Au cross section, we show the di-electron invariant mass distributions for unlike sign pairs ( $e^+e^-$ ), like sign pairs ( $e^+e^+$  or  $e^-e^-$ ) and the subtracted difference in Figure 1. The number of  $J/\psi$  counts for each centrality range is determined from the number of signal counts above "background" within a fixed invariant mass window. The PHENIX acceptance and Level-2 trigger efficiencies are the same within a few percent for unlike sign pairs and like sign pairs in the  $J/\psi$  mass region. Therefore, the sample of like sign pairs is a good representation with no additional scale factor of the "background" due to simple combinatorics.

In order to extract a  $J/\psi$  signal strength, we employ a counting method where we subtract from the number of unlike sign pairs the number of like sign pairs in the mass window  $2.8 < m < 3.4 \text{ GeV}/c^2$ . We have chosen a wide invariant mass window to be consistent with the signal extraction method from our proton-proton analysis [24], and to limit our sensitivity to the exact mass width value. Although we expect from our Monte Carlo studies a mass width of order 60 MeV, we cannot quantitatively verify this even with our proton-proton data sample due to low statistics. We note that in principle there is more in-

TABLE I: Statistical results for  $J/\psi$  counts are shown for three exclusive centrality ranges. Shown are the number of unlike and like sign counts within the mass window ( $2.8 < m < 3.4 \text{ GeV}/c^2$ ). Also shown are the most likely signal value with the 68% statistics confidence interval (for the peripheral and mid-central cases), and the 90% confidence level upper limits.

Centrality	Unlike Sign Counts	Like Sign Counts	Most Likely Signal	90% C.L.
00-20%	33	41	0	9.9
20-40%	16	8	$8_{-4.1}^{+4.8}$	14.4
40-90%	7	2	$5_{-2.6}^{+3.1}$	9.3

formation to be utilized in the exact distribution of the candidates within the mass window. However, we have found that this does not add to the significance of the result given the low counts and the lack of constraint on the  $J/\psi$  and background line shape.

Table I shows the number of unlike and like sign counts within the mass window. For given observed counts of  $N_l$  (like sign) and  $N_u$  (unlike sign), the likelihood  $L(\nu_l, \nu_u)$  for the expectation values  $\nu_l$  and  $\nu_u$  is given as

$$L(\nu_l, \nu_u) = \frac{\nu_l^{N_l} e^{-\nu_l}}{N_l!} \times \frac{\nu_u^{N_u} e^{-\nu_u}}{N_u!} \quad (1)$$

We then integrate  $L(\nu_l, \nu_u)$  to give the likelihood  $L(\nu_s)$  for the expectation value of the net signal counts  $\nu_s = \nu_u - \nu_l$

$$L(\nu_s) = \int_0^\infty \int_0^\infty L(\nu_l, \nu_u) \delta(\nu_s - \nu_u + \nu_l) d\nu_l d\nu_u \quad (2)$$

We show the likelihood distribution  $L(\nu_s)$  for the mid-central (20%-40%) events in Figure 2. Although  $L(\nu_s)$  is normalized such that  $\int_{-\infty}^\infty L(\nu_s) d\nu_s = 1$ , it has a non-zero probability for negative expected net signal value ( $\nu_s < 0$ ). Since the unlike sign contains *signal + background*, and the like sign contains only *background*, the only physically allowed values for  $\nu_s$  are greater than or equal to zero. Thus, we remove the probability range corresponding to  $\nu_s < 0$ , and re-normalize the remaining probability integral to one [25], as shown in the same Figure 2. We then determine for each centrality the 90% confidence level upper limit, and the 68% confidence interval around the most likely value for the peripheral and mid-central ranges. These values are shown in Table I.

Since the net signal is negative for the 0-20% central event class, we can only quote a 90% confidence level upper limit. Also, even for the 20-40% and 40-90% centrality classes, the signal observed is not significant at the two standard deviation level and thus we also show 90% confidence level upper limits for completeness. The limited statistical significance of the results is clear from the mass distributions shown in Figure 1.

In the intermediate mass region below the  $J/\psi$ ,  $2.0 < m < 2.8 \text{ GeV}/c^2$ , the shapes and absolute yield of like

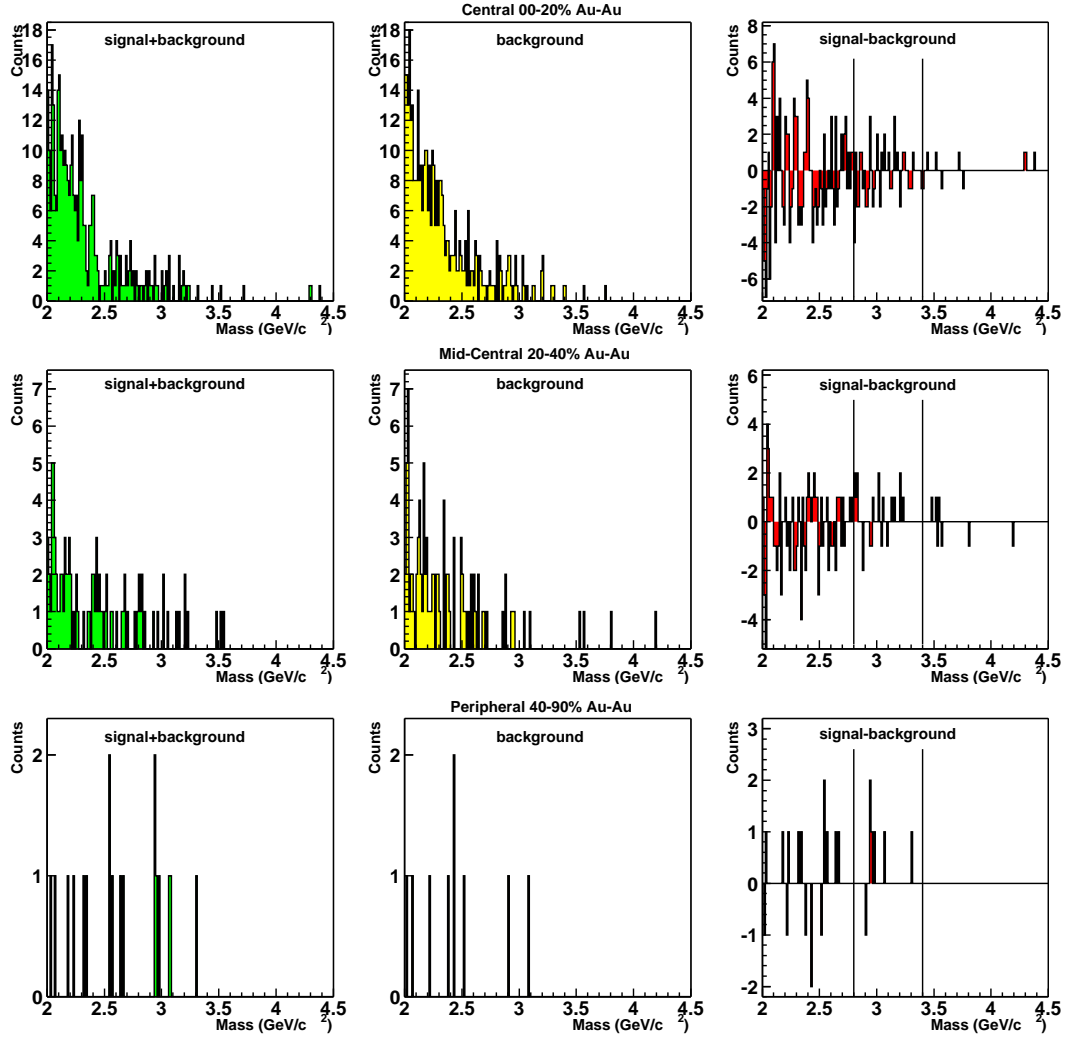


FIG. 1: (Color online) Dielectron invariant mass distribution in Au-Au reactions (top row: most central, 0-20% central, middle row: mid-central, 20-40% central, and bottom row: peripheral, 40-90% central) for unlike sign pairs containing signal+background (left column), like sign pairs containing only background (center column) and the subtracted difference (right column).

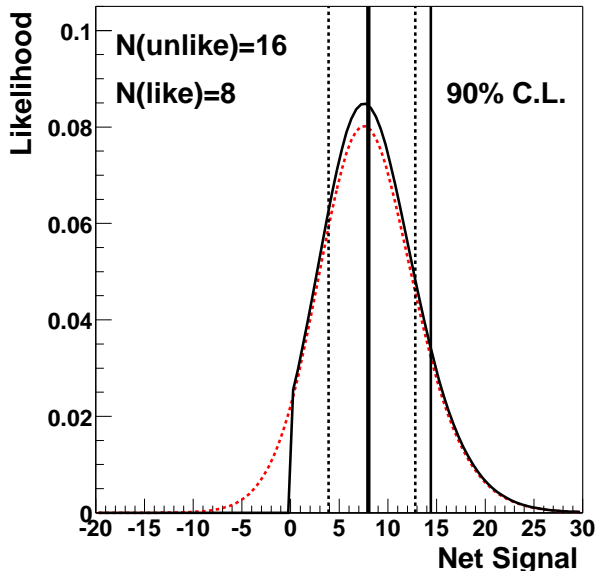


FIG. 2: (Color online) The Poisson statistical likelihood distribution as a function of the expected net signal. The distributions are for the mid-central case of  $N_{unlike}=16$  and  $N_{like}=8$ . The dashed curve is the likelihood distribution, and the black is after eliminating the unphysical net signal less than zero and re-normalizing. Vertical lines are shown to indicate the most likely value (8), the 68% confidence interval values, and the 90% confidence level upper limit.

sign and unlike sign dielectron mass distributions are well reproduced by an event mixing method within a few percent. This indicates that most of the dielectron pairs are from uncorrelated electron and positron candidates. They are originating from Dalitz decays, photon conversions, open charm/beauty semi-leptonic decays, and a small contamination of mis-identified hadrons. The unlike sign pairs should also have a component from semi-leptonic decays of charm and anti-charm pairs, but its

contribution is less than the statistical uncertainty of the data [26]. A complete analysis of the intermediate mass region will be presented elsewhere [27].

Our method of measurement does not separate contributions from decay feed-down from other states such as the  $\chi_c$  and  $\psi'$ , and thus our  $J/\psi$  counts include these feed down sources. Our acceptance and efficiency is identical for the resulting  $J/\psi$  from these decays as for prompt  $J/\psi$ , and thus they enter our signal weighted simply by their relative production and branching fraction into  $J/\psi + X$ . Another contribution may result from  $B$  meson decays into  $J/\psi$ . However, if we assume a  $b\bar{b}$  cross section in proton-proton reactions  $\sigma_{b\bar{b}} \approx 2 - 5 \mu\text{b}$  [28] and that beauty production scales with binary collisions, we would expect a contribution of order 1-4% relative to primary  $J/\psi$  or  $J/\psi$  from  $\chi_c$ . This percentage contribution calculation assumes that the primary  $J/\psi$  also scales with binary collisions. If primary  $J/\psi$  are substantially suppressed, the  $B$  meson decay contribution  $J/\psi$  would constitute a larger fraction of our measured  $J/\psi$ , especially at higher  $p_T$ .

It should also be noted that some signal in the unlike sign pairs from correlated open charm  $c\bar{c} \rightarrow D(\rightarrow e^+ + X) + \bar{D}(\rightarrow e^- + X)$  will contribute in our mass window. Assuming binary scaling in charm production with a proton-proton cross section  $\sigma_{c\bar{c}} \approx 650 \mu\text{b}$  [14], this contribution in the  $J/\psi$  mass region is estimated to be about 0.1 events in the 0-20%, 0.05 events in the 20-40%, and 0.02 events in the 40-90% centrality bins.

## V. $J/\psi$ YIELD CALCULATION

We quote our results as the branching fraction of  $J/\psi \rightarrow e^+e^-$  ( $B=5.93 \pm 0.10 \times 10^{-2}$  [25]) times the invariant yield at mid-rapidity  $dN/dy|_{y=0}$ . We calculate this quantity for three exclusive centrality ranges as detailed below.

$$B \frac{dN}{dy}|_{y=0} = \frac{N_{J/\psi}}{N_{mb-evt} + (\epsilon_{lvl2-eff} \times N_{lvl2-evt})} \times \frac{1}{\Delta y} \times \frac{1}{\epsilon_{acc-eff} \times \epsilon_{cent}} \quad (3)$$

The number of signal counts  $N_{J/\psi}$  from both the “minimum bias” and Level-2 triggered event samples are shown in Table I. The number of events from the “minimum bias” sample  $N_{mb-evt}$  is 25.9 million Au-Au events. The number of effective events sampled by the Level-2 trigger is  $(\epsilon_{lvl2-eff} \times N_{lvl2-evt})$ , which is the Level-2 trigger efficiency times the number of events processed by the Level-2 trigger, 23.4 million Au-Au events. This formulation appropriately weights the two data samples

by the expected number of  $J/\psi$ .

The efficiency of the Level-2 trigger  $\epsilon_{lvl2-eff}$  was determined by running the trigger algorithm on simulated  $J/\psi$  and carrying out a full offline reconstruction of the resulting electron-positron decay pair. The efficiency was calculated via counting the fraction of successfully reconstructed  $J/\psi$  events that were also found by the trigger. In these trigger simulations, the channel-by-channel calibrations for the RICH and EMC were used to convert

the simulated signals into realistic values representative of a specific period in the run, before passing them to the Level-2 trigger.

The overall  $J/\psi$  trigger efficiency from the trigger simulations was  $\epsilon_{lvl2-eff} = 0.75 \pm 0.04$ . The systematic error was determined by studying the dependence of the trigger efficiency on the collision vertex position, the assumed  $J/\psi$  transverse momentum and rapidity distribution, collision centrality, and the period of the run from which the channel-by-channel calibrations were taken. After evaluating all of the above dependencies, we assign a 5% systematic error to the  $J/\psi$  trigger efficiency.

The efficiency result from the trigger simulations was confirmed using real data in two ways. First, the minimum bias data sample in Au-Au collisions was analysed to calculate the  $J/\psi$  trigger efficiency. This was done by taking the ratio of the events that have an electron pair with invariant mass between 2.8 and 3.4 GeV/c<sup>2</sup> that fired the  $J/\psi$  trigger to all of the events having electron pairs in that invariant mass range. The trigger efficiency estimate from this check is  $0.67 \pm 0.10$  (stat). Second, the triggers were run on a sample of 26 events from the proton-proton data set that passed all of the  $J/\psi$  cuts in the offline analysis and had invariant masses between 2.8 and 3.4 GeV/c<sup>2</sup>. The Level-2  $J/\psi$  trigger accepted 19 of these events, yielding an estimate of  $0.73 \pm_{0.10}^{0.07}$  (stat), in very good agreement with the trigger simulation result. These results verify that the trigger performance is similar for real data and simulations.

The  $J/\psi$  acceptance and efficiency  $\epsilon_{acc-eff}$  is determined with a GEANT based Monte Carlo simulation of the PHENIX experiment. The detector response has been tuned to reproduce the resolution and performance of the real detector. The efficiency includes not only the tracking efficiency, but also the probability for passing all of the electron identification selection cuts. The electron identification efficiency determined by the Monte Carlo is verified by a clean electron sample from conversion photons. We also account for run by run efficiency changes by counting the relative number of reconstructed electrons and positrons per event in our data sample. We show the PHENIX acceptance and efficiency as a function of transverse momentum in Figure 3.

Since we do not have the statistics to determine the transverse momentum distribution of the  $J/\psi$ , we must employ a model for the  $p_T$  dependence to determine an overall acceptance and efficiency. We use two different functional forms for the  $p_T$  distributions to test the model sensitivity of our acceptance. We use an exponential in  $p_T$  and an exponential in  $p_T^2$  as motivated by fits to  $J/\psi$  data at lower energies [29]. The two models give similar acceptance values given a common  $\langle p_T \rangle$  value input. The largest uncertainty comes from the value of  $\langle p_T \rangle$  assumed. PHENIX has measured  $J/\psi$  production in proton-proton reactions at  $\sqrt{s} = 200$  GeV and finds a  $\langle p_T \rangle = 1.80 \pm 0.23$  (stat)  $\pm 0.16$  (sys) GeV/c [24]. We use this value to determine our acceptance and efficiency averaged over all  $p_T$ . The  $J/\psi$   $\langle p_T \rangle$  in Au-Au col-

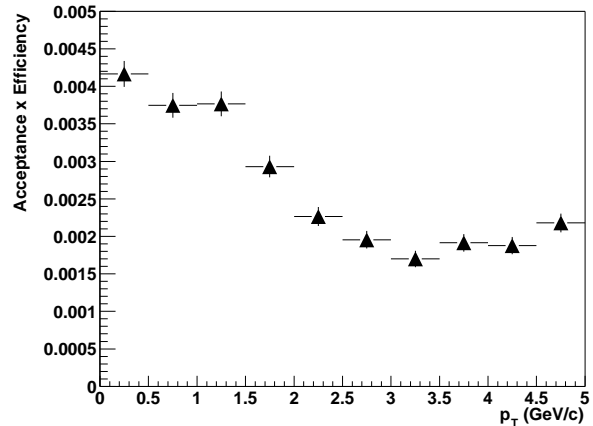


FIG. 3: The PHENIX  $J/\psi$  acceptance  $\times$  efficiency as a function of the  $J/\psi$  transverse momentum is shown. Most of the acceptance is with one lepton into each of the two PHENIX central spectrometers. This contribution peaks at  $p_T = 0$  and decreases with increasing  $p_T$ . The rise in the acceptance at high  $p_T$  is from contributions where both electron and positron are accepted into one of the PHENIX central spectrometers.

TABLE II: The  $J/\psi$  acceptance  $\times$  efficiency and the centrality dependent efficiency are shown for three exclusive Au-Au centrality event classes.

Centrality bin	$\epsilon_{acc-eff}$	$\epsilon_{cent}$
00-20%	$0.0027 \pm_{0.0005}^{0.0009}$ (sys)	$0.61 \pm 0.06$ (sys)
20-40%	"	$0.78 \pm 0.08$ (sys)
40-90%	"	$0.90 \pm 0.09$ (sys)

lisions may differ from that in proton-proton reactions. Therefore we vary the  $\langle p_T \rangle$  from 1.0 to 3.0 GeV/c to determine our model dependent systematic errors. We assume that the  $J/\psi$  rapidity distribution is flat over the range  $-0.35 < y < 0.35$  where we measure. The final value for the  $J/\psi$  acceptance and efficiency is shown in Table II. This acceptance and efficiency has a 20% systematic error from uncertainties in matching the Monte Carlo to the detector response, a 10% systematic error from run-to-run variation corrections, and a  $\pm_{24}^{32}\%$  systematic error from the uncertainty in the  $\langle p_T \rangle$ .

Our tracking and electron identification efficiencies exhibit a centrality dependence due to overlapping hits and energy contamination in the calorimeter. We determine this dependence by embedding Monte Carlo  $J/\psi$  into real data events of different centrality selections. The corresponding efficiency factor  $\epsilon_{cent}$  varies from 56% for the 0-5% most central events to 98% for the 85-90% most peripheral events.

The final values for the embedding efficiency in our wide centrality bins are sensitive to the true centrality dependence of the  $J/\psi$  production. In order to estimate the systematic error due to this uncertainty we assume two

different centrality dependence models: (1) binary collision scaling and (2) participant collision scaling. Within our centrality ranges, we find that these two models yield less than a 5% difference and we include this in our systematic error. We assign an additional 10% systematic error to account for uncertainties in the Monte Carlo embedding procedure. The centrality dependent efficiency values are shown in Table II.

In our  $B dN/dy$  calculation, we have added the systematic errors from all of the contributing factors in quadrature and find +35% and -41% total systematic error on the invariant yield in each of the centrality ranges. The dominant systematic error results from the uncertainty in the  $\langle p_T \rangle$  of the  $J/\psi$  distribution.

## VI. RESULTS

The  $B dN/dy|_{y=0}$  values for the three exclusive centrality selections are shown in Table III. We have calculated using a Glauber model [21] the number of expected participating nucleons  $N_{part}$  and the number of

expected binary collisions  $N_{coll}$  for each centrality range. These results are shown in Table IV, in addition to the  $B dN/dy|_{y=0}$  values divided by the expected number of binary collisions.

TABLE III: We show the statistically most likely  $J/\psi$  invariant yield ( $B dN/dy|_{y=0}$ ) value and the 68% confidence interval for peripheral (40-90%) and mid-central (20-40%) collisions. We also show the 90% confidence level upper limit and the systematic error on this limit for all three different centrality ranges of Au-Au collisions.

Centrality	$B dN/dy _{y=0} (\times 10^{-4})$	
	Most Likely Value	90% C.L.U.L.
00-20%	N.A.	6.08+1.56 ( <i>sys</i> )
20-40%	4.00 <sup>+2.34</sup> <sub>-2.01</sub> ( <i>stat</i> ) <sup>+1.36</sup> <sub>-1.60</sub> ( <i>sys</i> )	7.19 + 2.43 ( <i>sys</i> )
40-90%	0.86 <sup>+0.52</sup> <sub>-0.44</sub> ( <i>stat</i> ) <sup>+0.29</sup> <sub>-0.35</sub> ( <i>sys</i> )	1.60 + 0.54 ( <i>sys</i> )

The PHENIX result for the  $J/\psi$  invariant yield in proton-proton induced reactions at  $\sqrt{s}=200$  GeV at mid-rapidity [24] is

$$B dN/dy|_{y=0}(pp) = 1.46 \pm 0.23 (stat) \pm 0.22 (sys) \pm 0.15 (abs) \times 10^{-6} \quad (4)$$

The systematic error (abs) represents the uncertainty of the normalization of the total proton-proton invariant yield.

We show in Figure 4 the results from the three Au-Au centrality bins and the proton-proton data normalized per binary collision as a function of the number of participating nucleons. Note that for proton-proton reactions, there are two participating nucleons and one binary collision.

## VII. DISCUSSION

Despite the limited statistical significance and systematic uncertainty of these first  $J/\psi$  results, we can address some important physics questions raised by the numerous theoretical frameworks in which  $J/\psi$  rates are calculated.

We show in Figure 5 binary scaling expectations as a gray band. We also show a calculation of the suppression expected from “normal” nuclear absorption using a  $\sigma_{c\bar{c}-N} = 4.4$  mb [30] and 7.1 mb [6, 31]. A recent measurement in proton-nucleus collisions at lower energies [30] favors the smaller absorption cross section, thus underscoring the importance of measuring  $J/\psi$  in proton(deuteron)-nucleus collisions at RHIC energies. We also show the NA50 suppression pattern relative to binary scaling [3], normalized to match our proton-proton data point at 200 GeV. The data disfavor binary scaling,

while they are consistent with “normal” nuclear absorption alone and also the NA50 suppression pattern measured at lower energies, within our large statistical errors.

One model calculation [16] including just the “normal” nuclear and plasma absorption components at RHIC energies is shown in Figure 6. The higher temperature ( $T$ ) and longer time duration of the system at RHIC lead to a predicted larger suppression of  $J/\psi$  relative to binary collision scaling. This specific model [16], and in general this class of models [8, 32], cannot be ruled out at this time due to our null result (90% confidence level upper limit) for the most central collisions.

Many recent theoretical calculations also include the possibility for additional late stage re-creation or coalescence of  $J/\psi$  states. In [16], they include both break-up and creation reactions  $D + \bar{D} \leftrightarrow J/\psi + X$ . At the lower fixed target CERN energies, this represents a very small contribution due to the small charm production cross section. However, at RHIC energies, where in central Au-Au collisions there are of order 10  $c\bar{c}$  pairs produced, the contribution is significant. The sum of the initial production, absorption, and re-creation as shown in Figure 6 is also consistent with our experimental data.

A different calculation [15] assumes the formation of a quark-gluon plasma in which the mobility of heavy quarks in the deconfined region leads to increased  $c\bar{c}$  coalescence. This leads to a very large enhancement of  $J/\psi$  production at RHIC energies for the most central

TABLE IV: We show the number of participating nucleons and the number of binary collisions for three different centrality ranges of Au-Au collisions, and the associated systematic errors. We show the statistically most likely value for the  $J/\psi$  invariant yield ( $B dN/dy|_{y=0}$ ) divided by the expected number of binary collisions for peripheral (40-90%) and mid-central (20-40%) collisions. We also show the 90% confidence level upper limit and the systematic error on this limit for all three different centrality ranges of Au-Au collisions. The systematic error in the invariant yield per binary collision does not include the systematic error in the expected number of binary collisions. This error contribution is negligible for the central and mid-central categories and would increase the systematic error for the peripheral category by 6%.

Centrality	$N_{part}$	$N_{coll}$	$B dN/dy _{y=0}$ per binary collision ( $\times 10^{-6}$ )	
			Most Likely Value	90% C.L.U.L.
00-20%	$280 \pm 4$	$779 \pm 75$	N.A.	$0.78 + 0.20 (sys)$
20-40%	$140 \pm 5$	$296 \pm 31$	$1.35^{+0.79}_{-0.68} (stat)^{+0.46}_{-0.54} (sys)$	$2.43 + 0.82 (sys)$
40-90%	$34 \pm 3$	$45 \pm 7$	$1.91^{+1.15}_{-0.97} (stat)^{+0.65}_{-0.77} (sys)$	$3.55 + 1.21 (sys)$

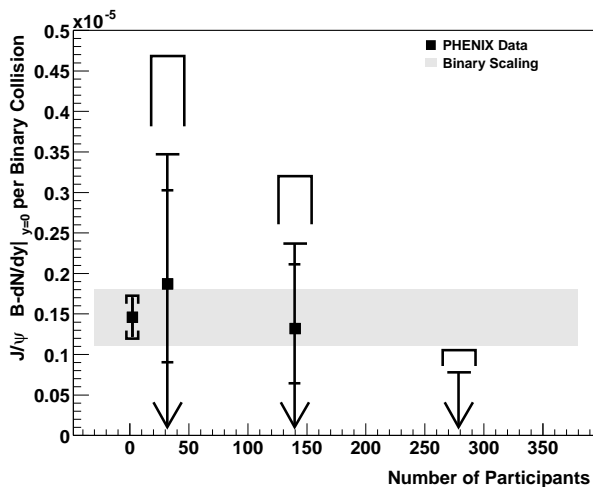


FIG. 4: The  $J/\psi$  invariant yield per binary collision is shown for proton-proton reactions and three exclusive centrality ranges of Au-Au reactions all at  $\sqrt{s_{NN}} = 200$  GeV. For the proton-proton reactions, we show the most likely value as a data point (square), the statistical error, and the estimated systematic errors as brackets. For the three Au-Au data points, we show as arrows the 90% confidence level upper limits. The bracket above the limit includes the estimated systematic error on these limits. In the case of the peripheral and mid-central ranges, we also show, as a square marker, the statistically most likely value and as two horizontal dashes the 68% confidence interval. The gray band indicates binary scaling and the width is the quadrature sum of the statistical and systematic error on our proton-proton data point. For the Au-Au points, the systematic error in the invariant yield per binary collision does not include the systematic error in the expected number of binary collisions. This error contribution is negligible for the central and mid-central categories and would increase the systematic error for the peripheral category by 6%.

reactions. The model considers the plasma temperature ( $T$ ) and the rapidity width ( $\Delta y$ ) of charm quark production as input parameters. Shown in Figure 6 are the calculation results for  $T = 400$  MeV and  $\Delta y = 1.0, 2.0, 3.0, 4.0$ . The narrower the rapidity window in which all charm quarks reside, the larger the probability for  $J/\psi$

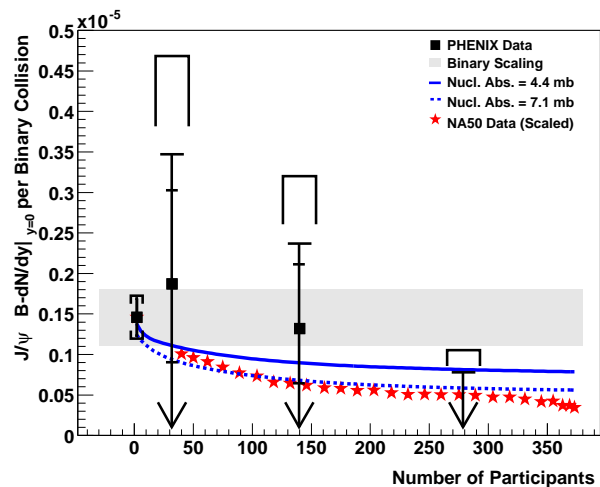


FIG. 5: (Color online) The  $J/\psi$  invariant yield per binary collision is shown from proton-proton reactions and three exclusive centrality ranges of Au-Au reactions all at  $\sqrt{s_{NN}} = 200$  GeV. The lines are the theoretical expectations from “normal” nuclear absorption with  $\sigma_{c\bar{c}-N} = 4.4$  mb (solid curve) and 7.1 mb (dashed curve) cross section. The stars are the  $J/\psi$  per binary collision measured by the NA50 experiment at lower collision energy. In order to compare the shapes of the distribution, we have normalized the NA50 data to match the central value for our proton-proton results.

formation.  $\Delta y = 1.0$  is consistent with the three dimensional spherically symmetric thermal distribution, and results in a charm yield at midrapidity that is inconsistent with the PHENIX preliminary charm yield as determined from single electron measurements [14].  $\Delta y = 4.0$  is consistent with expectations from factorized QCD and PYTHIA with CTEQ5L structure functions [13]. All of these parameters within this model predict a  $J/\psi$  enhancement relative to binary collisions scaling, which is disfavored by our data.

Another framework for determining quarkonia yields is to assume a statistical distribution of charm quarks that may then form quarkonia. A calculation assuming thermal, but not chemical equilibration [17] is shown in Figure 6, and is also consistent with our data.

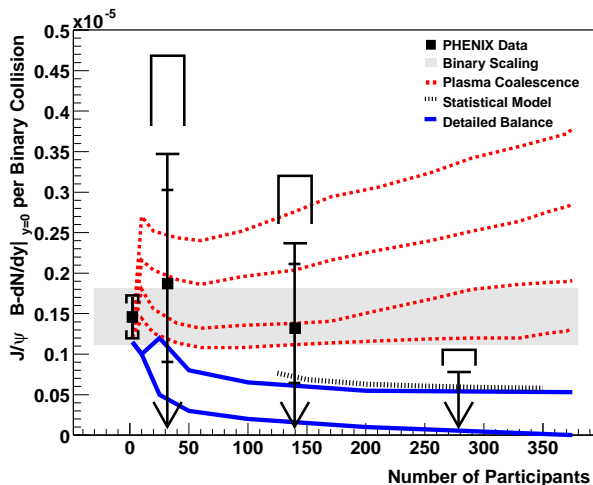


FIG. 6: (Color online) The  $J/\psi$  invariant yield per binary collision is shown from proton-proton reactions and three exclusive centrality ranges of Au-Au reactions all at  $\sqrt{s_{NN}} = 200$  GeV. The lowest curve is a calculation including “normal” nuclear absorption in addition to substantial absorption in a high temperature quark-gluon plasma [16]. The curve above this is including backward reactions that recreate  $J/\psi$ . The statistical model [17] result is shown as a dotted curve for mid-central to central collisions just above that. The four highest dashed curves are from the plasma coalescence model [15] for a temperature parameter of  $T = 400$  MeV and charm rapidity widths of  $\Delta y = 1.0, 2.0, 3.0, 4.0$ , from the highest to the lowest curve respectively.

Significantly larger data sets are required to address the various models that are still consistent with our first measurement. Key tests will be the  $p_T$  and  $x_F$  dependence of the  $J/\psi$  yields, and how these compare with other quarkonium states such as the  $\psi'$ .

### VIII. SUMMARY

PHENIX has shown first results on  $J/\psi$  production in Au-Au collisions at  $\sqrt{s_{NN}} = 200$  GeV at mid-rapidity as measured via electron-positron pairs. We find that models that predict  $J/\psi$  enhancement relative to binary

collision scaling are disfavored, while we cannot discriminate between various scenarios leading to suppression relative to binary scaling.

This first measurement from PHENIX will be followed with high statistics measurements in both the electron channel at midrapidity and at forward and backward rapidities in the PHENIX muon spectrometers. Such measurements are expected in the next few years and will address the full range of heavy quarkonia production and evolution models.

### Acknowledgments

We thank the staff of the Collider-Accelerator and Physics Departments at Brookhaven National Laboratory and the staff of the other PHENIX participating institutions for their vital contributions. We acknowledge support from the Department of Energy, Office of Science, Nuclear Physics Division, the National Science Foundation, Abilene Christian University Research Council, Research Foundation of SUNY, and Dean of the College of Arts and Sciences, Vanderbilt University (U.S.A), Ministry of Education, Culture, Sports, Science, and Technology and the Japan Society for the Promotion of Science (Japan), Conselho Nacional de Desenvolvimento Científico e Tecnológico and Fundação de Amparo à Pesquisa do Estado de São Paulo (Brazil), Natural Science Foundation of China (People’s Republic of China), IN2P3/CNRS and Commissariat à l’Energie Atomique (France), Bundesministerium fuer Bildung und Forschung, Deutscher Akademischer Austausch Dienst, and Alexander von Humboldt Stiftung (Germany), Hungarian National Science Fund, OTKA (Hungary), Department of Atomic Energy and Department of Science and Technology (India), Israel Science Foundation (Israel), Korea Research Foundation and Center for High Energy Physics (Korea), Russian Academy of Science, Ministry of Atomic Energy of Russian Federation, Ministry of Industry, Science, and Technologies of Russian Federation (Russia), VR and the Wallenberg Foundation (Sweden), the U.S. Civilian Research and Development Foundation for the Independent States of the Former Soviet Union, the US-Hungarian NSF-OTKA-MTA, the US-Israel Binational Science Foundation, and the 5th European Union TMR Marie-Curie Programme.

- 
- [1] T. Matsui, H. Satz, Phys. Lett. B **178**, 416 (1986).  
[2] F. Karsch, Lect. Notes Phys. **583**, 209 (2002).  
[3] NA50 Collaboration, M.C. Abreu *et al.*, Phys. Lett. B **477**, 28 (2000). M.C. Abreu *et al.* (NA50 Collaboration), Phys. Lett. B **521**, 195 (2001).  
[4] E866-FNAL Collaboration, M. Leitch *et al.*, Phys. Rev. Lett. **84**, 3256 (2000).  
[5] F. Arleo *et al.*, Phys. Rev. C **61**, 054906 (2000).  
[6] D. Kharzeev *et al.*, Z. Phys. C **74**, 307 (1997).  
[7] H. Fujii and T. Matsui, Phys. Lett. B **545**, 82 (2002).  
[8] J.P. Blaizot, P.M. Dinh, J.Y. Ollitrault, Phys. Rev. Lett. **85**, 4012 (2000).  
[9] X.-M. Xu, C.-Y. Wong, T. Barnes, Phys. Rev. C **67**, 014907 (2003). T. Barnes, E.S. Swanson, C.-Y. Wong, X.-M. Xu, nucl-th/0302052.  
[10] N. Armesto *et al.*, Nucl. Phys. A **698**, 583 (2002). A. Capella and D. Sousa, nucl-th/0303055.  
[11] J. Qiu, J.P. Vary, X. Zhang, Phys. Rev. Lett. **88**, 232301 (2002).  
[12] A.K. Chaudhuri, nucl-th/0207082.  
[13] K. Adcox *et al.*, Phys. Rev. Lett. **88**, 192303 (2002).  
[14] PHENIX Collaboration, R. Averbeck *et al.* Nucl. Phys.

- A715**, 252c (2003).
- [15] R.L. Thews, M. Schroedter, J. Rafelski, Phys. Rev. C **63**, 054905 (2001). R.L. Thews, Strange Quark Matter 2003 conference proceedings.
- [16] L. Grandchamp, R. Rapp. Nucl. Phys. **A709**, 415 (2002). L. Grandchamp, R. Rapp, Phys. Lett. B **523**, 60 (2001).
- [17] A. Andronic *et al.*, nucl-th/0303036.
- [18] N. Hammon *et al.*, Phys. Rev. C **59**, 2744 (1999).
- [19] K. Adcox, Nucl. Instr. and Meth. **A499**, 469 (2003).
- [20] M. Chiu *et al.*, Phys. Rev. Lett. **89**, 012302 (2002).
- [21] S.S. Adler *et al.*, nucl-ex/0304022, submitted to Phys. Rev. Lett.
- [22] J.T. Mitchell *et al.*, Nucl. Instr. and Meth. **A482**, 491 (2002).
- [23] Y. Akiba *et al.*, Nucl. Instr. and Meth. Phys. Res. **A433**, 143 (1999).
- [24] S.S. Adler *et al.*, submitted to Phys. Rev. Lett. [hep-ex/0307019].
- [25] K. Hagiwara *et al.* (Particle Data Group), Phys. Rev. D **66**, 010001 (2002).
- [26] PHENIX Collaboration, J.L. Nagle *et al.*, Nucl. Phys. **A715**, 695c (2003).
- [27] PHENIX Collaboration, in preparation.
- [28] C.H. Jaroschek, "A Study of Bottom Productin with the PYTHIA Event Generator", Masters Thesis, State University of New York at Stony Brook (2001).
- [29] M.H. Schub *et al.*, Phys. Rev. D **52**, 1307 (1995).
- [30] B. Alessandro *et al.* (NA50 Collaboration), Phys. Lett. B **553**, 167 (2003).
- [31] J.L. Nagle, M.J. Bennett, Phys. Lett. **B 465**, 21 (1999).
- [32] S. Digal *et al.*, Phys. Lett. B **549**, 101 (2002).